CHAPTER II

BACKGROUND AND LITERATURE REVIEWS

2.1 The Basic Principles of Semiconductor

As part of the growing awareness and concern about a sustainable planet, a big effort has been directed to green practices and environmental remediation in the industry and human activities in general. Several methods and approaches have been used to accomplish this task, and one of the most promising is heterogeneous photocatalysis using semiconductor nanoparticles (Fox and Dulay, 1993; Linsebigler *et al.*, 1995; Herrmann, 1999; Hoffmann *et al.*, 1999; Rajeshwar, 1995). Large band gap oxide semiconductor materials (TiO_2; WO_3; ZnO; CdS) for photocatalysis show advantages such as stability (chemical inertness and photostability), non-toxicity and low cost. In addition, many of these materials exhibit catalytic activity after repeated photocatalytic cycles and can be recovered using physical methods once the reaction is completed without significant loses (Fox and Dulay, 1993). These advantages make semiconductor photocatalysis a real and promising method in attaining the goal for a clean and better environment. However, one of the disadvantages in the use of these materials is that ultraviolet (UV) light is required for photoexitation with attendant electrical energy costs (Herrmann, 1999; Hoffmann *et al.*, 1995).

Some special criteria have to be met in the choice of the semiconductor for a particular reaction. The standard reduction potential of the acceptor species must be more positive than the potential of the conduction band edge of the semiconductor surface in order to let the reduction reaction by the conduction band electrons to occur. On the other hand, to begin an oxidation process by the valence band holes, the standard reduction potential of the donor must be more negative than the potential corresponding to the valence band edge of the semiconductor surface. A comparison between the band edge positions of some semiconductors versus the standard hydrogen electrode (SHE) is illustrated in Figure 2.1, as well as the band gap energies of some semiconductor.

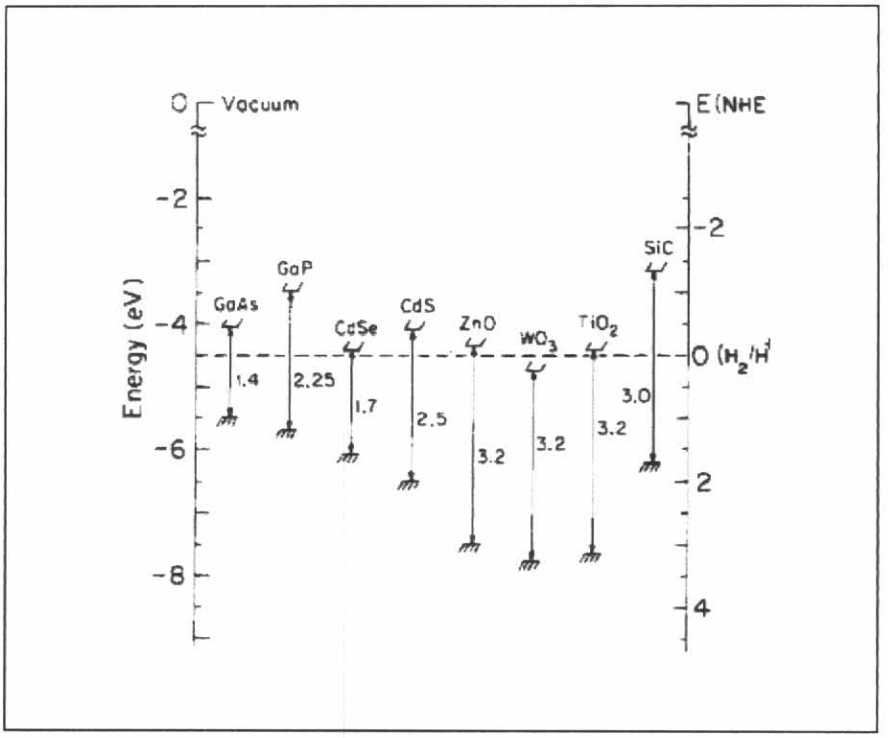

Figure 2.1 Band edge positions and band gap energies for some semiconductors. (Linsebigler *et al.*, 1995)

2.2 Titanium Dioxide (TiO_2)

Titanium dioxide, also known as titania, is an important commercial product that has been used in various commercial applications that range from industrial (paint and pigment), to cosmetic (skin-care products). On a research level, this material has attracted interest for water splitting (Fujishima and Honda, 1972), solar photovoltaic cells and water or air remediation (Linsebigler *et al.*, 1995; Rajeshwar, 1995; Thompson and Yates, 2006). This metal oxide has been used as a potential photocatalyst of choice for the total destruction (mineralization) of organic pollutants in air and water. As mentioned earlier, this semiconductor material has high activity and stability to light illumination, and also has non-toxic and widely occurring component elements (Rajeshwar, 1995; Thompson and Yates, 2006).

TiO_2 belongs to a family of transition metal oxides. It occurs in nature in three crystalline forms: anatase, rutile and brookite. Both rutile and anatase crystallize in the tetragonal system and brookite in the rhombic system. Crystallographic

information on the three polymorphs of TiO_2 is summarized in Table 2.1 and the crystallographic structures are shown in Figure 2.2

Anatase and rutile are the commonly occurring forms of TiO_2. At normal pressure, rutile is the thermodynamically stable form of TiO_2 at all temperatures; it is about 1.2 – 2.8 kcal/mol more stable than anatase (Finklea, 1983). Anatase, the meta-stable polymorph, transforms rapidly to rutile at temperatures above 700 ^{0}C. The phase change from anatase to rutile has been reported to occur in different temperature ranges from 600 – 1000 ^{0}C depending on the crystallite size and impurity contents. Both anatase and rutile are wide band gap semiconductors in which a filled valence band derived from the O 2p orbitals is separated from an empty conduction band derived from the Ti 3d orbitals. The energy band gaps of anatase and rutile are 3.2 eV and 3.0 eV respectively.

Table 2.1 Comparison of the properties of different polymorphs of titanium dioxide.

	Rutile	**Anatase**	**Brookite**
Formula weight	79.890	79.890	79.890
Z	2	4	8
Crystal system	Tetragonal	Tetragonal	Orthorhombic
Point group	4/mmm	4/mmm	mmm
Space group	P42/mmm	I41/amd	Pbca
Unit cell			
a(Å)	4.5845	3.7842	9.184
b(Å)	-	-	5.447
c(Å)	2.9533	9.5146	5.145
Volume	62.07	136.25	257.38
Molar volume	18.693	20.156	19.377
Density	4.2743	3.895	4.123

Sources: (http://ruby.colorado.edu/~smyth/min/tio2.html)

The anatase phase has a higher photocatalytic activity than the rutile counterpart. The photocatalytic activity is better because the crystal structure, size distribution, porosity, band gap, band edge position, surface defects, surface hydroxyl group and surface area of anatase are different from rutile (Milnes and Feucht, 1973; Palmisano *et al.*, 1997). The energy band structure and surface chemistry are the key factors in photoactivity. The band gap energy of anatase (3.2 eV) corresponds to UV light (388 nm) while the band gap energy of rutile (3.0 eV) corresponds to violet light (413 nm). The difference in band gap comes from the level of conduction band of anatase which is higher than that of rutile by about 0.2 eV. Thus the electrons from the conduction band of anatase have higher reducing power than rutile.

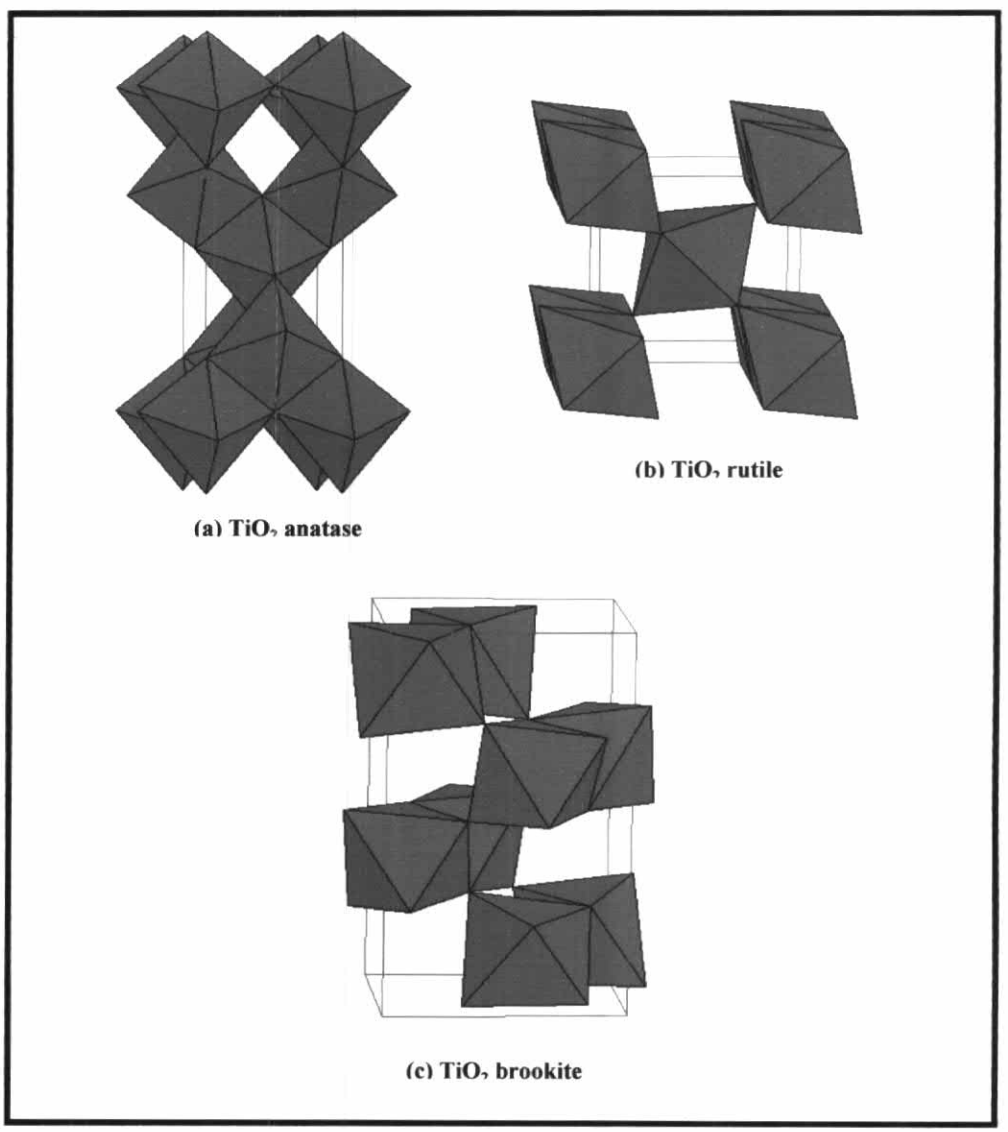

Figure 2.2 Crystal structure of TiO_2 : (a) anatase (b) rutile and (c) brookite (http://ruby.colorado.edu/~smyth/min/tio2)

On the other hand, the powder form of TiO_2 is generally used as the photo-catalyst. However, it has several problems (Lee *et al.*, 2003): (1) Separation of the catalyst from suspension after the reaction is difficult. (2) The suspended particles tend to aggregate at high concentrations. (3) The amount applied is small and limited. (4) The efficiency was limited by turbidity effect. Consequently the field of semiconductor electrochemistry and photoelectrochemistry has evolved from the use of semiconductor single crystals to polycrystalline thin films, mesoporous films, nanostructure films and, more recently nanotube films distinguished. Among these films, nanotubes are of great interest due to their high surface-to-volume ratio and size-dependent properties, oriented perpendicular to the substrate, unusual electronic transport and mechanical strength characteristics.

Several recent studies have indicated that titania nanotube have improved properties compared to any other forms of titania for application in photocatalysis (Adachi *et al.*, 2000; Chu *et al.*, 2003), sensing (Varghese *et al.*, 2003; Varghese *et al.*, 2004; Mor *et al.*, 2004), and photoelectrolysis (Mor, Shankar *et al.*, 2004; Mor *et al.*, 2005). Titania nanotubes arrays has been fabricated by various approaches such as template synthesis, hydrothermal reaction, spray pyrolysis (Wang *et al.*, 2004; Hoyer, 1996; Chen *et al.*, 2005) and anodization of titanium in fluoride-based baths (Cai *et al*, 2005; Beranek *et al.*, 2003; Mor *et al.*, 2003; Sul *et al.*, 2001; Varghese *et al.*, 2005; Mor *et al.*, 2006). However, of these nanotube fabrication routes, the architecture demonstrating by far the most remarkable properties are highly ordered nanotube arrays made by anodization of titanium in fluoride-base baths the dimension of which can be precisely controlled and processes occur at low temperature and at atmospheric pressure.

2.3 Fabrication of titania nanotube arrays by anodization

Tailoring the structure and morphology of semiconductor materials on a nanometer size range has fundamental and practical importance (Alivisatos, 1996). Nanotubular semiconductor structures are particularly of interest because of their unusual electronic transport and mechanical strength characteristics. For illustrative purposes, the simplistic view of electron transport through a self assembled nanorod layer may be contrasted with a nanostructured (mesoporous) semiconductor counterpart (Figure 2.3). Arguably, the injected electrons at one end of the layers (from a nanoparticulate layer photoexcited dye, for example) experience a much less tortuous path in the semiconductor nanorod assembly than in the random, unaligned layer. The shorter transit time also translates to lower recombination losses and higher photon-to-electron conversion efficiency.

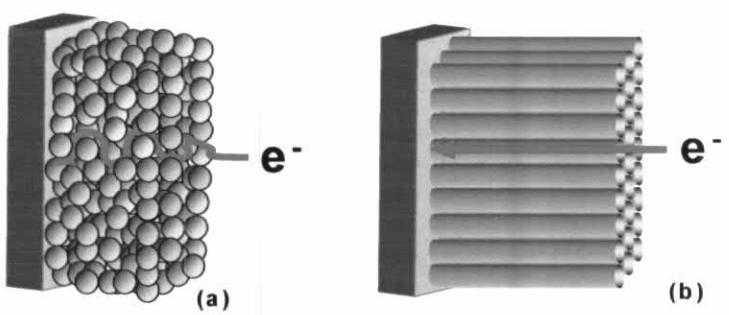

Figure 2.3 Schematic comparison of electron transport in (a) a mesoporous and (b) a self assembled nanorod layer.

Spurred by these and other considerations, a variety of materials in nanotubular or nanorod form have been prepared and, in many cases, considered for solar energy conversion applications including oxide semiconductors such as ZnO (Li *et al.*, 2000) and TiO_2 (de Tacconi *et al.*, 2006).

Interest in TiO_2 nanotube arrays stems long standing interest in this rather amazing material dating back to 1980 (Rao *et al.*, 1980). As mentioned above, titanium dioxide nanotubes and nanotube arrays have been the subject of recent studies in other laboratories. In these studies, templates derived from 'track-etch' polymer membranes, anodic alumina or polystyrene (latex) spheres were deployed to

house TiO_2 nanotubes and nanowires using either solution (e.g., sol-gel) chemistry or electrodeposition. However, template-free approaches are rather more versatile for growing 1-D semiconductor structures. Thus, TiO_2 hollow fibers were prepared from supramolecular precursor assemblies (Kobayashi *et al.*, 2000). Nanotubes of TiO_2 were synthesized by hydrothermal treatment (Kasuga *et al.*, 1998; Chen *et al.*, 2002) for example, of crystalline TiO_2 particles with aqueous NaOH (Kasuga *et al.*, 1998). Using a seed layer of ZnO nanorods on Si substrate, aligned TiO_2 nanotube and nanowire arrays were prepared by liquid phase deposition (Lee *et al.*, 2005). Aligned rutile and anatase TiO_2 nanorods as well as anatase TiO_2 nanowalls were synthesized by a template- and catalyst-free metal organic chemical vapor deposition (Wu *et al.*, 2004). Finally, a seed layer of TiO_2 nanoparticles on Ti foil was used to prepare large oriented arrays and continuous films of TiO_2-based nanotubes (Tian *et al.*, 2003).

The formation of self-assembled nanotube arrays is a complex phenomenon comprising of delicate balances between anodic film growth, chemical corrosion, electrochemical corrosion, and field-driven mass transport of various species (Taveira *et al.*, 2005). Considerable information exists on the mechanistic aspects of anodic alumina growth dating back to more than 50 years (Mei *et al.*, 2005). On the presumption that similar phenomena apply to valve metals such as titanium, the first stage is barrier layer oxide growth on the Ti substrate. Formation of this compact layer decreases the electric field abruptly; the main reaction in this regime (called the "recovery" period) is chemical dissolution. After a certain time, the barrier layer thickness decreases increasing the electric field across this layer. Now the field-assisted oxide growth and electrochemical dissolution can kick in. Thus uniform titania nanotube arrays were reported by anodic oxidation of Ti in HF electrolyte (Gong *et al.*, 2001). Subsequently, another research group also reported the formation of long nanotubes during anodization of titanium in neutral fluoride solutions (Beranek *et al.*, 2003). More recent efforts by these two groups have sought to increase the nanotube length and also address the mechanistic aspects of nanotube formation and growth; reviews are available (Mor *et al.*, 2006; Grimes, 2007). Such TiO_2 nanotube arrays have been used by several groups for dye-sensitized solar cells (Macák, *et al.*, 2005; Wei *et al.*, 2006).

2.3.1 Mechanistic of nanotube array formation

The key processes responsible for anodic formation of nanoporous alumina and titania appear to be the same, and are fundamental to the formation of straight titania nanotubes. The surface of titanium metals is even and smooth after being polished carefully. However, the surface is covered with a compact thin oxide film due to the intrinsic property of valve metal (Choi *et al.*, 2004)

The step formations are:

Step 1 Oxide growth at the surface of the metal occurs due to interaction of the metal with O^{2-} or OH^- ions (Varghese and Grimes, 2004). After the formation of an initial oxide layer, these anions migrate through the oxide layer reaching the metal/oxide interface where they react with the metal. Indicates the compact oxide begins to dissolve and dissolution takes place only in selective area. The overall reactions for anodic oxidation of titanium can be represented as

$$2H_2O \longrightarrow O_2 + 4e^- + 4H^+ \qquad \text{(Eq. 2.1)}$$

$$Ti + O_2 \longrightarrow TiO_2 \qquad \text{(Eq. 2.2)}$$

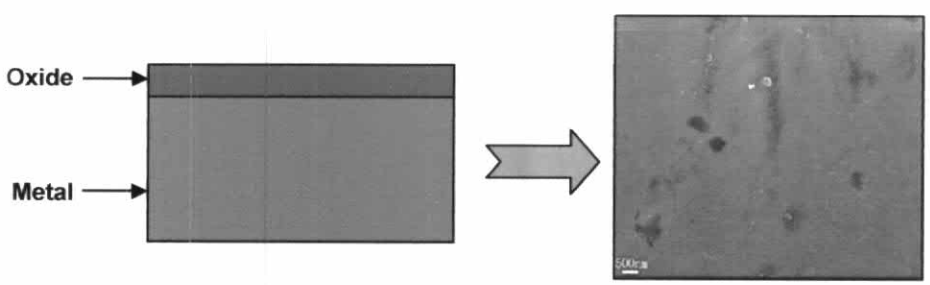

Figure 2.4 Oxide layer formations.

Step 2 The compact oxide film at the titanium surface existed with or without the assistance of electric field and HF solution can etch the oxide quickly. But the etching speed was different at different area of the oxide due to the different stress on the surface of oxide film which was called selective etching. Metal ion (Ti^{4+}) migration from the metal at the metal/oxide interface; Ti^{4+} cations will be ejected from the metal/oxide interface under application of an electric field that move towards the oxide/electrolyte interface. Small pits formed due to the localized dissolution of the oxide, represented by the following reaction:

$$TiO_2 + 6F^- + 4H^+ \longrightarrow TiF_6^{2-} + 2H_2O \qquad \text{(Eq. 2.3)}$$

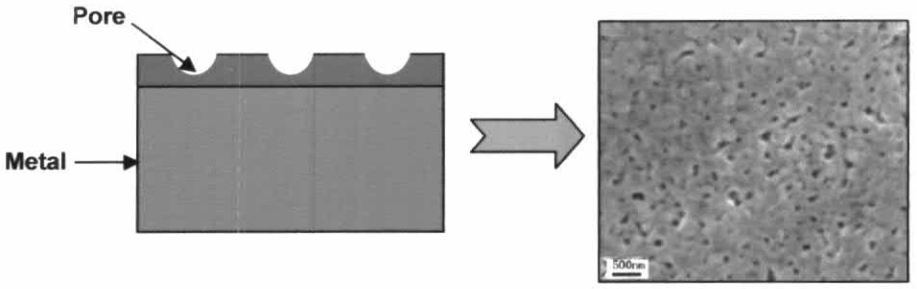

Figure 2.5 Pore formations (fluoride addition) during anodization.

Step 3 Field assisted dissolution of the oxide at the oxide/electrolyte interface (Parkhutik and Shershulsky, 1992; Macdonald, 1993). Due to the applied electric field the Ti–O bond undergoes polarization and is weakened promoting dissolution of the metal cations. Ti^{4+} cations dissolve into the electrolyte, and the free O^{2-} anions migrate towards the metal/oxide interface to interact with the metal (Siejka and Ortega, 1977; Thompson, 1997). These pits convert into bigger pores and the pore density increases. After that, the pores spread uniformly over the surface. The pore growth occurs due to the inward movement of the oxide layer at the pore bottom (barrier layer).

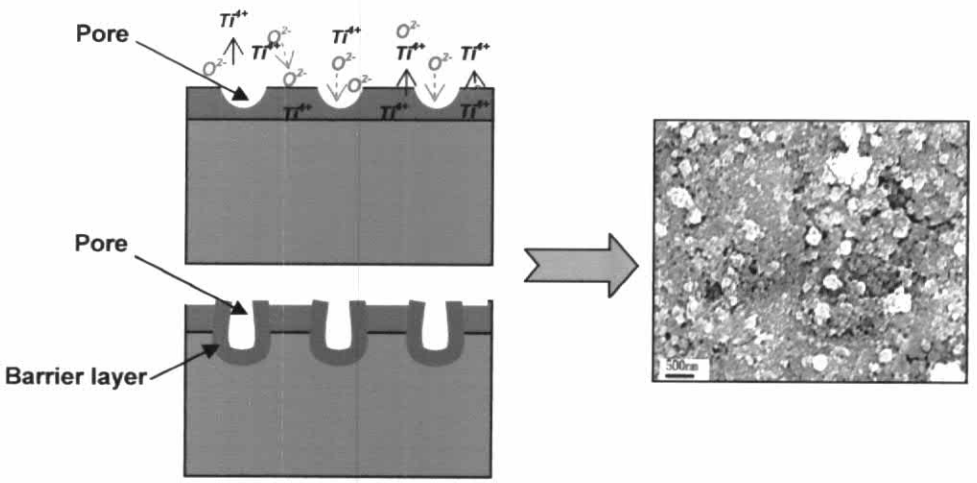

Figure 2.6 Growth of the pores due to filed assistant dissolution of titanium.

Step 4 Chemical dissolution of the metal, or oxide, by the acidic electrolyte also takes place during anodization. Chemical dissolution of titania in the HF electrolyte plays a key role in the formation of nanotubes rather than a nanoporous structure (Wu *et al.*, 2000). The rate of oxide growth at the metal/oxide interface and the rate of oxide dissolution at the pore-bottom/electrolyte interface ultimately become equal; thereafter the thickness of the barrier layer remains unchanged although it moves further into the metal making the pore deeper. As the pores become deeper, the electric field in these metallic regions increases, enhancing the field-assisted oxide growth and oxide dissolution, and the interpores voids start forming.

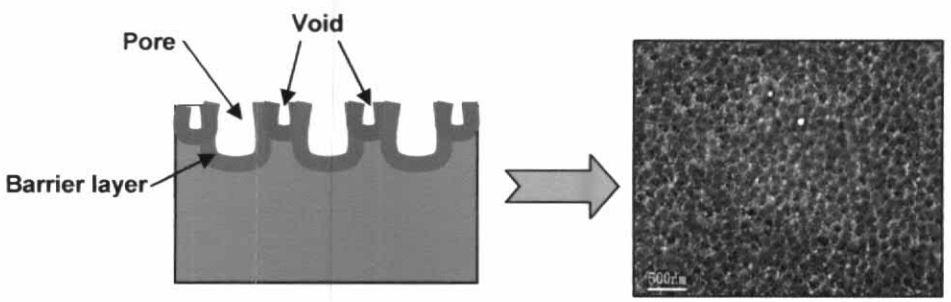

Figure 2.7 Void formations in metallic part between the pores.

Step 5 Fully developed nanotube array with a corresponding top view. Both voids and tubes grow in equilibrium to finally yield a tubular structure. If the titanium oxide either in the wall or at the pore bottom dissolves at a balance rate, the pore depth keeps constant and does not change with anodizing time (Chen *et al.*, 2006). As determined for a given electrolyte concentration and anodization potential. This chemical dissolution, the key for the self-organized formation of the nanotube arrays, reduces the thickness of the oxide layer (barrier layer) keeping the electrochemical etching (field-assisted oxidation and dissolution) process active.

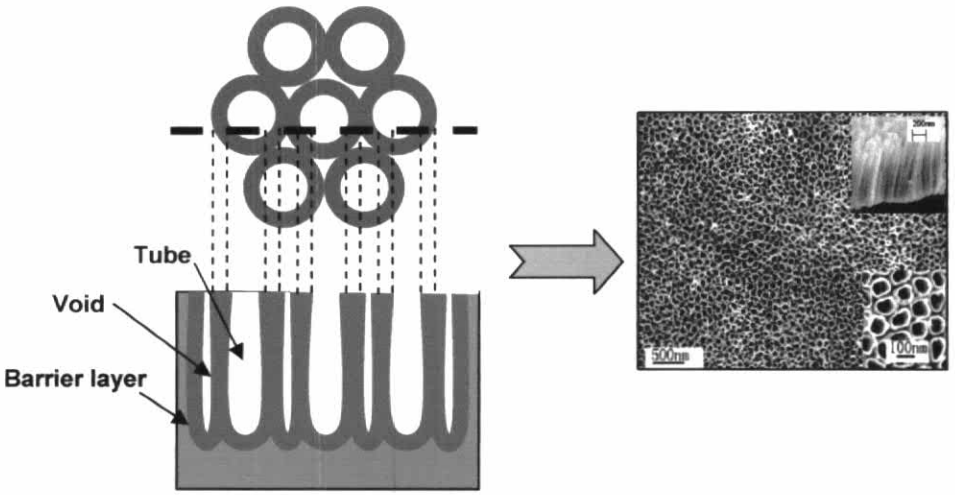

Figure 2.8 Formation of nanotubes of titanium.

2.3.2 Conventional anodization VS Pulse anodization

The formation of TiO_2 nanotube array is determined by the balance between the electrochemical oxidization and the chemical dissolution (Varghese *et al.*, 2005). When the electrochemical oxidization proceeds faster than the chemical dissolution, the barrier layer grows, which in turn reduces the electrochemical oxidization process to the rate determined by the chemical dissolution. The chemical dissolution rate determines the nanotubes length and the potential window in which nanotubes can be formed. However the nanotubes can not be formed if the chemical dissolution is too high or too low is difficult to maintain and if the rapid oxide formation the pores were not uniform and internal cracks of the oxide film, nanotubes clump, or lean together, presenting crack-like features apparent in the surface because of dielectric break down (Varghese *et al.*, 2005; Mor *et al.*, 2006).

These previous anodization studies (de Tacconi *et al.*, 2006; Mor *et al.*, 2006) have used either constant potential (potentiostatic) or constant current (galvanostatic) nanotube growth modes. On the other hand, the interplay of electrochemical and chemical processes inherent in the anodic film growth suggests that pulsing the potential between carefully chosen limits and varying the duty cycle (i.e., voltage 'on' and 'off' durations) can exert an important influence on the film morphology and nanotube formation. Pulse anodization with different pulse periods and different

cathodic potentials and keeping constant the anodization potential (namely 20 V, based in previous data that afforded best performance in photocurrent and morphology). Depending on the potential of the cathodic pulse the effect of chemical reactions (with electrolyte components) could be observed due to the cancellation of the electrochemical oxidation reactions. At that condition the chemical reactions solely play its role in the nanotube structure formation and without interference of the electrochemical reactions. Thus by adjusting the pulse time at negative or zero potential should be detecting the effect of the electrolyte on the nanotube wall thickness and nanotube diameter. By balancing the electrochemical and chemical reactions through adjustment of the time periods at low potential to allow chemical reactions to perform alone.

In summary, the pulse anodization approach offers a new, hitherto unavailable dimension in fine control and tuning of anodic layer growth and nanotube self-assembly on targeted metal substrates. Note that this approach is compatible with both the constant voltage and current growth modes (Figure 2.9 and 2.10). From a practical process economics perspective, pulse anodization also offers savings in energy consumption relative to the continuous process counterpart. In this dissertation research, pulse anodization is shown to result in better-defined nanotube morphologies than in the constant voltage growth mode. The resultant TiO_2 nanotube arrays show a higher quality of photoresponse than those grown via the continuous anodization route. Important mechanistic insights are also furnished by these data. Careful tuning of the pulse duty cycle and the negative voltage limit points toward the importance of *chemical* (corrosion) processes during nanotube growth as well as surface passivation effects introduced by the adsorption of electrolyte species (e.g., NH_4^+) on the growing oxide nanotube arrays and pulse anodization strategy affords an expeditious route to doping of the nanotube host by judicious choice of the negative voltage limit and the electrolyte composition.

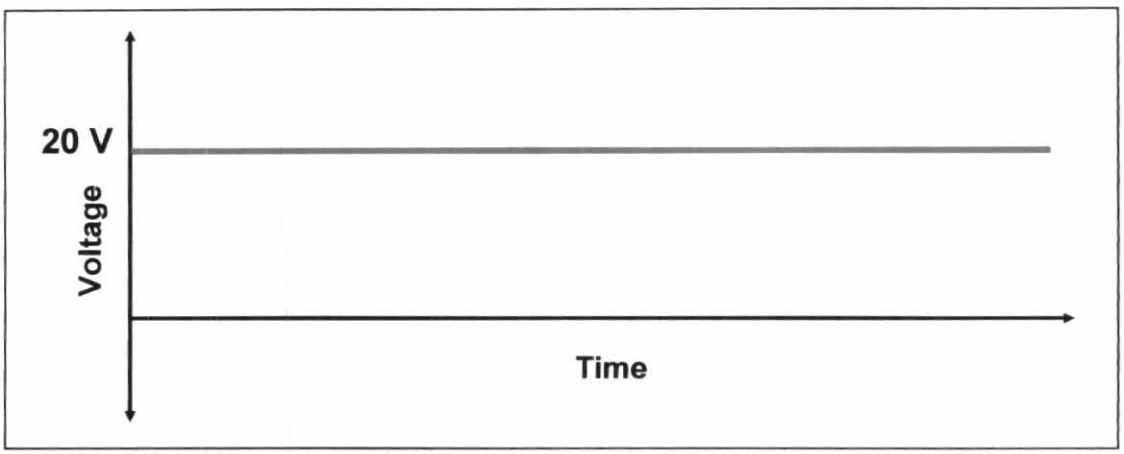

Figure 2.9 Constant potential used for anodic growth of TiO_2 nanotube.

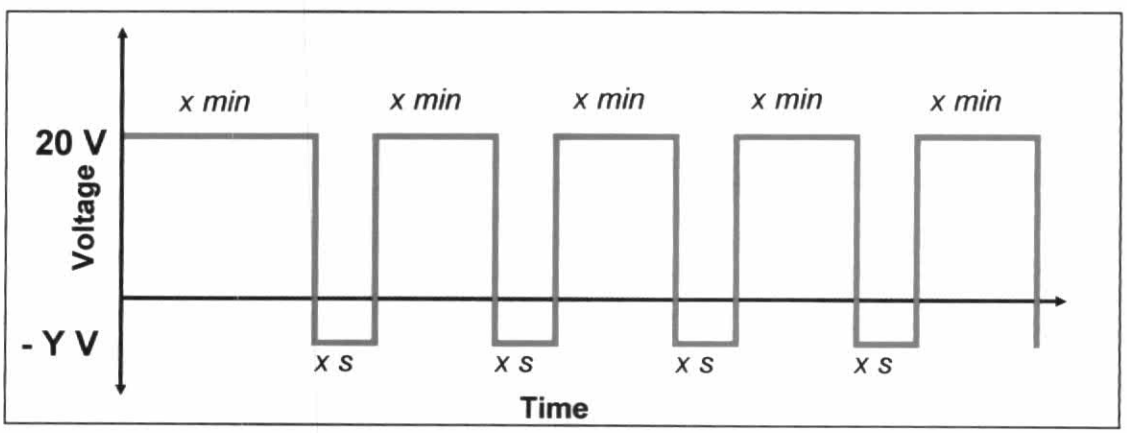

Figure 2.10 Potential pulse waveform used for anodic growth of TiO_2 nanotube.

2.4 Doped titania nanotube

2.4.1 Electron Energy Levels in Semiconductors

The solid is an array of atoms with each atom having different electronic energy states. When these atoms come closer to form the solid, these energy states overlap resulting in energy bands (Yildiz *et al.*, 1989). The electrons previously accommodated in the electronic energy levels are now accommodated in energy bands. The energy band containing bonding (valence) electrons is termed the valence band. The band next higher in energy to the valence band is termed the conduction band. The energy difference (E_g) between the valence band and the conduction band determines whether the solid is a conductor, semiconductor or an insulator (Figure 2.11).

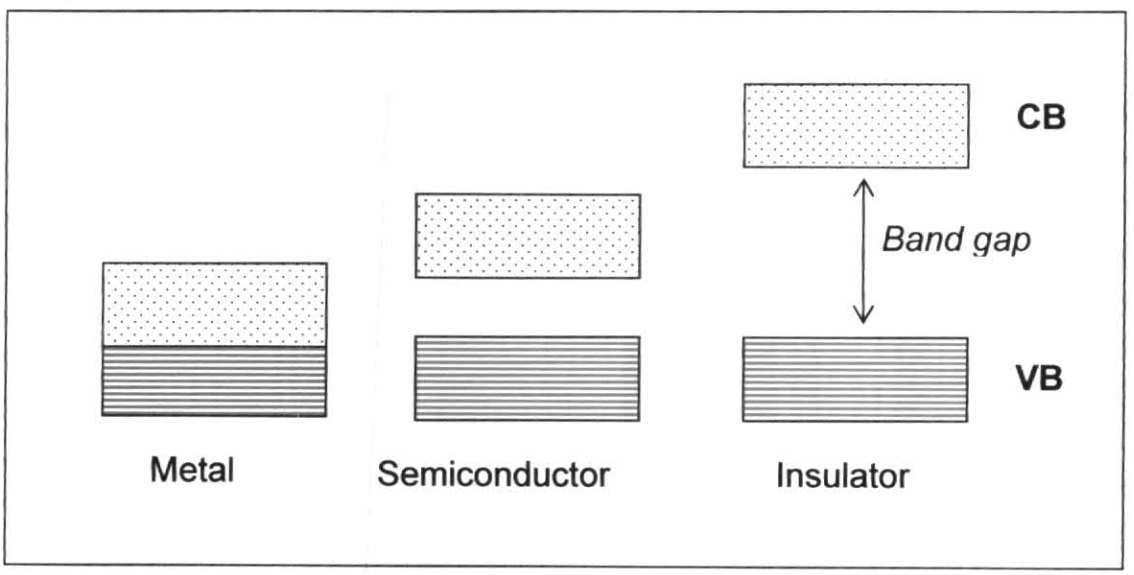

Figure 2.11 Energy band structures for metal, semiconductor and insulator materials.

When the conduction and valence bands of a conductor overlap or lie closer, valence electrons can easily get excited into the conduction band. This will give a flow of mobile electrons (under an electric field) resulting in good electrical conductivity. An insulator has large band gap energy. Therefore the electrons in the valence band cannot easily get excited into the conduction band. Having no mobile electrons, an insulator does not exhibit electrical (i.e., electronic) conductivity under normal conditions.

The energy difference between the valence and the conduction bands in a semiconductor is in between those in a conductor and an insulator. Although $E_g > kT$ for most semiconductors at ordinary temperatures, there are still some thermally excited carriers in the conduction band which give conduction, i.e., for semiconductors typically have band gap in the 1 eV-4eV range (Table 2.2), if the band gap is not so large, electrons can move into the conduction band.

Table 2.2 Some elemental and compound semiconductors for Photoelectrochemical application

Semiconductor	Conductivity type(s)	Optical band gap energy (eV)[a]
Si	n, p	1.11
GaAs	n, p	1.42
GaP	n, p	2.26
InP	n, p	1.35
CdS	n	2.45
CdSe	n	1.70
CdTe	n, p	1.50
TiO_2	n	3.00 (rutile) 3.20 (anatase)
ZnO	n	3.35

[a] The values quoted are for the bulk semiconductor.

The promotion of electrons leaves a positively charged vacancy in the valence band which is referred to as a hole. These holes can be moved through space by the transfer of an electron to the vacancy, and therefore holes are considered to be mobile and opposite in polarity to electrons. Electrons can be excited to the conduction band either thermally or photochemically. However there is another method for generating charge carriers (i.e., electrons or holes) within a semiconductor, referred to as doping.

2.4.2 Doped semiconductor

Doping involves the addition of a different element into the semiconductor. Undoped semiconductors are referred to as intrinsic semiconductors (Figure 2.12).

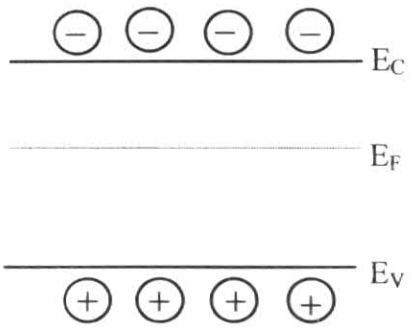

Figure 2.12 Schematic diagram of the energy levels of an intrinsic semiconductor.

Doped semiconductors in which the dominant charge carriers are electrons are referred to as n-type semiconductors, whereas those in which holes are majority charge carriers are referred to as p-type semiconductors (Figure 2.13).

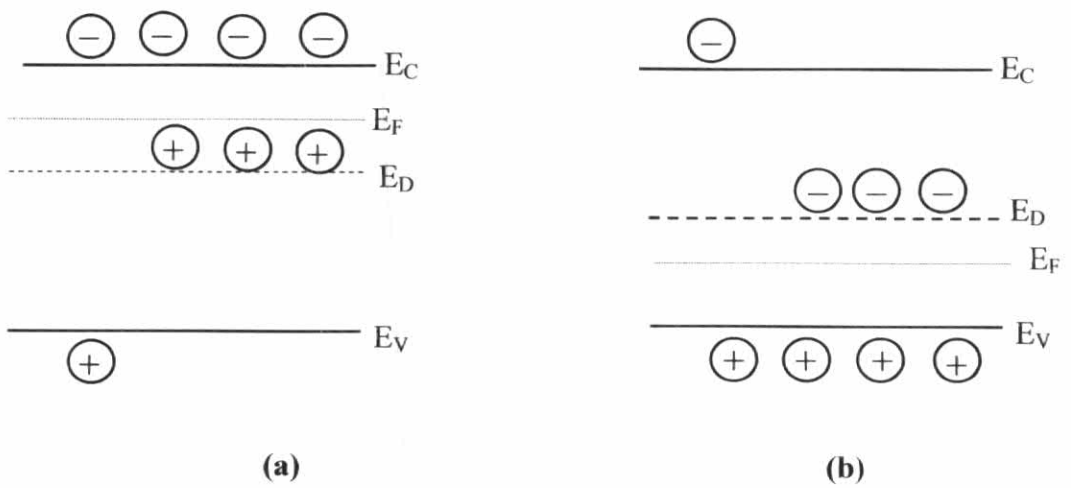

Figure 2.13 Schematic diagram of the energy levels of (a) n-type semiconductor (b) p-type semiconductor. E_F is the so-called Fermi level.

Another important concept in discussion of solid state materials is the Fermi level, E_F. This is defined as the energy level at which the probability of occupation by an electron is 0.5(at 0 K); for example, for an intrinsic semiconductor the Fermi level lies approximately at the mid point of the band gap (Figure 2.12). Doping changes the distribution of electrons within the solid, and hence changes the Fermi level. For an n-type semiconductor the Fermi level lies just below the conduction band, whereas for a p-type semiconductor it lies just above the valence band (Figure 2.13). In addition, as with metal electrodes, the Fermi level of a semiconductor electrode varies with the applied potential; for example a negative bias potential will "raise" the Fermi level.

2.4.3 Doped and metal-modified oxide nanotubes

In spite of its many positive attributes as a photoelectrode material, TiO_2 does suffer from poor solar photon conversion efficiency because of its rather wide band gap (3.0-3.2 eV). Consequently, only a very small fraction (~5%) of the overall solar spectrum can be harnessed by this material. Attempts at extending the visible light response of TiO_2 by metal doping date back to ~1977 (Augustynsk *et al.*,1977; Ghosh and Maruska, 1977). These and many subsequent studies of doping of TiO_2 have been reviewed by Rajeshwar and Hoffman (Rajeshwar, 1985 ; Rajeshwar, 2007 ; Rajeshwar, in press; Hoffman, 1995).

A recent innovation in this topic has been the incorporation into TiO_2 of non-metallic elements such as fluorine, carbon, nitrogen, and sulphur. As with the trend with metal dopants, very few of the studies in Table 2.3. Other than the desired optical response, non-metallic dopants also exert electronic effects on the host behaviour as with the metal dopants. Thus F-doping is observed to cause a reduction in the $e^- - h^+$ recombination rate (Hoffman *et al.*, 1995) while N-doping at high levels has the opposite effect and serves to suppress the photocatalytic activity of the TiO_2 host. Conflicting views exist on non-metal doping, particularly with respect to the mechanistic aspects (Irie *et al.*, 2003).

Studies oriented toward doping of TiO_2 *nanotube arrays* have also begun to appear, notably from three research groups (Mor *et al.*, 2006; Grimes *et al.*, 2007). Thus, nitrogen was introduced into amorphous and crystalline (anatase) TiO_2

nanotube by ion implantation (Ghicov *et al.*, 2005). Subsequent work by the same group have reported on N-doping via ammonia decomposition in situ (Macák *et al.*, 2006). More recently, the photoresponse of TiO_2 nanotubes has been extended to the visible range by Cr-doping (Ghicov *et al.*, 2007). The Grimes group reports both carbon and fluorine incorporation during flame annealing of TiO_2 nanotubes. Nitrogen doping was reported by this group via the use of ammonium and nitrate ion containing electrolytes. The precise doping mechanism was reported to be "currently unclear, and the subject of ongoing studies" (Mor *et al.*, 2006).

Table 2.3 Representative studies on doping of TiO_2 with non-metallic elements

Entry No.	Title of article	Comments	Reference
1	Visible-Light Photocatalysis in Nitrogen-Doped Titanium Oxides	Both films and powders considered. Substitutional doping with nitrogen shown to bring about band gap narrowing and also high photocatalytic activity with visible light. Experimental data supported with first-principles calculations.	Asahi *et al.* 2001
2	Band Gap Narrowing of Titanium Dioxide by Sulfur Doping	Oxidative annealing of TiS_2 used. Ab initio calculations also reveal mixing of S 3p states with the valence bond to bring about band gap narrowing.	Umebayashi *et al.*, 2002
3	Efficient Photochemical Water Splitting by a Chemically Modified n-TiO_2	Combustion of Ti metal in a natural gas flame done to substitute carbon for some of the lattice oxygen sites. The photocatalysis performance data have been questioned (see Refs. 93-95).	Khan *et al.*, 2002
4	Daylight Photocatalysis by Carbon-Modified Titanium Dioxide	Titanium tetrachloride precursor hydrolyzed with nitrogen bases to yield (surprisingly) C-doped (instead of N-doped) TiO_2. Study oriented toward environmental remediation applicability.	Sakthivel and Kisch, 2003
5	Carbon-Doped Anatase TiO_2 Powders as a Visible-Light Sensitive Photocatalyst	Oxidative annealing of TiC used to afford yellow doped powders. Study focus as in Entry 5.	Irie *et al.*, 2003(a)
6	Nitrogen-Concentration Dependence on Photocatalytic Activity of $Ti_{2-x}N_x$ Powders	Samples prepared by annealing anatase TiO_2 under NH_3 flow at 550-600 °C.	Irie *et al.*, 2003(b)
7	Visible-Light Induced Hydro-philicity on Nitrogen-Substituted Titanium Dioxide Films	Degree of hydrophilicity correlated with the extent of substitution of nitrogen at oxygen sites.	Irie *et al.*, 2003(c)
8	Spectral Photoresponses of Carbon-Doped TiO_2 Film Electrodes	Raman spectra used to identify disordered carbon in the flame-formed samples in addition to lower nonstoichiometric titanium oxides identified by X-ray diffraction.	Noworyta and Augustynski, 2004
9	Photoelectrochemical Study of Nitrogen-Doped Titanium Dioxide for Water Oxidation	One of the few studies probing the influence of doping on OER.	Torres *et al.*, 2004
10	Metal Ion and N Co-doped TiO_2 as a Visible-Light Photocatalyst	Co-doped samples prepared by polymerized complex or sol-gel method. Doped N species found to reside at interstitial lattice positions in the host.	Sakatani *et al.*, 2004

From pulse anodization strategy, presented in the preceding section, affords an expeditious route to doping of the nanotube host by judicious choice of the negative voltage limit and the electrolyte composition. A variety of metals such as Ru, Rh, Pt, Pd etc. can be used for this purpose as reviewed by Rajeshwar (Rajeshwar, 2007) and Heller (Heller, 1981; Heller, 1984).

2.5 Applications of titania nanotube array

2.5.1 Heterogeneous Photocatalysis reaction of TiO_2 nanotube arrays

The processes of heterogeneous photocatalysis that occur on an illuminated semiconductor particle can be summarized shortly as follows (Figure 2.14) (Litter, 1999). As mentioned earlier, a semiconductor is characterized by an electronic band structure in which the highest occupied energy band, called valence band (VB) and the lowest empty band called conduction band (CB) are separated by a band gap. When a photon of energy higher or equal to the band gap energy is absorbed by a semiconductor particle, an electron (e^-) from the VB is promoted to the CB creating a positive hole (h^+) in the VB. This electron-hole pair formation is a key step in the photocatalytic process. The electron in the conduction band (e^-_{CB}) and the hole in the valance band (h^+_{VB}) can recombine on the surface or in the bulk of the particle by the emission of heat or can be trapped in surface states where they can react with donor (D) or acceptor (A) species adsorbed or close to the surface of the particle. Thus subsequent anodic and cathodic redox reactions can be initiated.

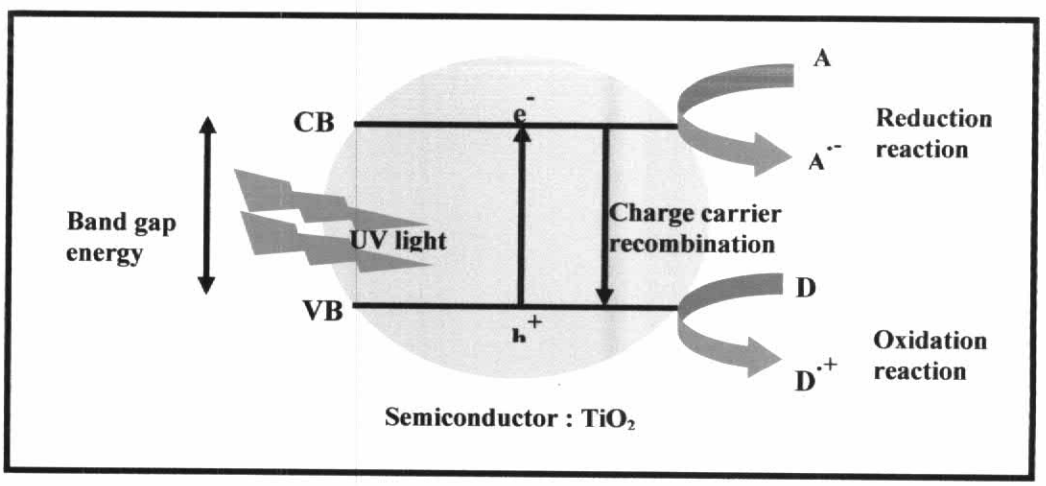

Figure 2.14 Schematic diagram of the heterogeneous photocatalytic process occurring on an illuminated semiconductor particle.

The energy level at the bottom of the CB is actually the reduction potential of photoelectrons and the energy level at the top of the VB determines the oxidizing ability of the photoholes. From the thermodynamic point of view, adsorbed redox species can be reduced photocatalytically by CB electrons if they have redox potentials more positive than the CB level of the semiconductor, and can be oxidized by VB holes if they have redox potentials more negative than the VB edge of the semiconductor.

2.5.1.1 Mechanism of TiO_2 Based Heterogeneous Photocatalysis

1) Charge carrier generation:

$$TiO_2 + h\nu \longrightarrow h^{+}_{VB} + e^{-}_{CB} \qquad \text{(Eq. 2.4)}$$

2) Charge carrier trapping:

$$h^{+}_{VB} + >Ti^{IV}OH \longrightarrow \{>Ti^{IV}OH^{\bullet}\}^{+} \qquad \text{(Eq. 2.5)}$$

$$e^{-}_{CB} + >Ti^{IV}OH \longrightarrow >Ti^{III}OH \qquad \text{(Eq. 2.6)}$$

3) Charge carrier recombination:

$$h^{+}_{VB} + >Ti^{III}OH \longrightarrow >Ti^{IV}OH \qquad \text{(Eq. 2.7)}$$

$$e^{-}_{CB} + \{>Ti^{IV}OH^{\bullet}\}^{+} \longrightarrow >Ti^{IV}OH \qquad \text{(Eq. 2.8)}$$

4) Interfacial charge transfer:

$$\{>Ti^{IV}OH^{\bullet}\}^{+} + D \longrightarrow >Ti^{IV}OH + D^{\bullet+} \qquad \text{(Eq. 2.9)}$$

$$\{>Ti^{III}OH\} + A \longrightarrow >Ti^{IV}OH + A^{\bullet-} \qquad \text{(Eq. 2.10)}$$

$>Ti^{IV}OH$ represents the primary hydrated surface functionality of TiO_2, $\{>Ti^{IV}OH^{\bullet}\}^{+}$ is the surface trapped valence band hole (i.e., surface bound hydroxyl radical) and $\{>Ti^{III}OH\}$ is the surface trapped conduction band electron (Hoffmann *et al.*, 1995).

2.5.1.2 Photocatalytic reaction of Chromium (VI) by TiO_2

Many researches agree that titanium dioxide is the best photocatalysis for environmental application at present. Advantage of titanium dioxide over other semiconductors are: 1) high activity, 2) large stability to light illumination, 3) low price, 4) nontoxicity. Illumination of TiO_2 by light with energy larger than the bandgap energy elevates electron in the valence band to the conduction band. The positive hole oxidizes either pollutant directly or water to produce OH radical whereas the electron in the conduction band reduces metal adsorbed to TiO_2 and then cause reduction and oxidation reactions. From this phenomena is available on TiO_2 photocatalysis for environmental application.

Interesting heavy metal is chromium because of the potential health risk from water contaminated with hexavalent chromium, local and federal regulations have been placed to increase public awareness and expand the standards for control of this pollutant nationwide. Today, almost every city has its own regulations for levels of Cr (VI) in drinking water, and analyses are made on a daily basis (Kimbrough *et al.*, 1999). Sources for contamination with this form of chromium are found in different industrial activities such as ore refining, chemical and refractory processing, cement-producing plants, automobile brake lining and catalytic converters for automobiles, leather tanneries, and chrome pigments also contribute to the atmospheric contribution of chromium. (USEPA, 1998). The metal chromium is used mainly for making steel and other alloys (ATSDR, 1998). Chromium compounds, in either the chromium (III) or chromium (VI) forms, are used for chrome plating, the manufacture of dyes and pigments, leather and wood preservation, and treatment of cooling tower water. Smaller amounts are used in drilling mud, textiles, and toner for copying machines (ATSDR, 1998).

Hexavalent (Cr(VI)) and trivalent (Cr(III)) represent the two primary oxidation states found in the environment. Cr(VI) presents a high carcinogenic risk, high solubility, and high mobility, while the trivalent form has relatively low toxicity, mobility and solubility. Use of physical or chemical remediation methods like adsorption, ion exchange or precipitation does not help in the efficient removal of the toxic hexavalent chromium from water. Instead, treatment and remediation is based

on reduction to the less soluble Cr(III). The most popular of these methods makes use of a strong reducing agent followed by the base precipitation as hydroxide. Other methods use direct current (Pamukcu *et al.*, 2004), Fe(II)/Fe(III) reaction (Hug *et al.*, 1997), or photocatalysis using titania (Chenthamarakshan *et al.*, 2000; Lin et al., 1993). The photocatalytic method is possible because transformation from Cr(VI) to Cr(III) can be driven as a photoassisted reduction under UV (or visible) illumination in aqueous suspensions using TiO_2 (Chenthamarakshan *et al.*, 2000).

There are many studied reported on photocatalytic reduction of Cr(VI) using TiO_2. The optimum conditions to treat chromium using TiO_2 was well established from the previous works (Kajitvichyanukul and Watcharenwong, 2005; Ku and Jung, 2001) It was found that Cr (VI) was well removed from wastewater at the reaction pH of 3. The photocatalytic reduction rate of Cr(VI) was found to be linearly increased with light intensity until a certain optimum light intensity was reached (Ku and Jung, 2001). At low pH, Cr(VI) exists in aqueous solution as the dichromate anion ($Cr_2O_7^{2-}$) which can be transformed to Cr(III) as shown in the equation:

$$Cr_2O_7^{2-} + 14H^+ + 6e^- \longrightarrow 2Cr^{3+} + 7H_2O \qquad \text{(Eq. 2.11)}$$

The reduction is possible because the standard potential for ($Cr_2O_7^{2-}$) /Cr^{3+} is 1.232 V Vs. SHE (Chenthmarakshan *et al.*, 2000; Harris, 2003), and this value is more positive than the potential of the conduction band edge of the titania semiconductor surface (Figure 2.15). The photogenerated holes oxidize water molecules to O_2 while the electrons reduce Cr(VI) to Cr(III).

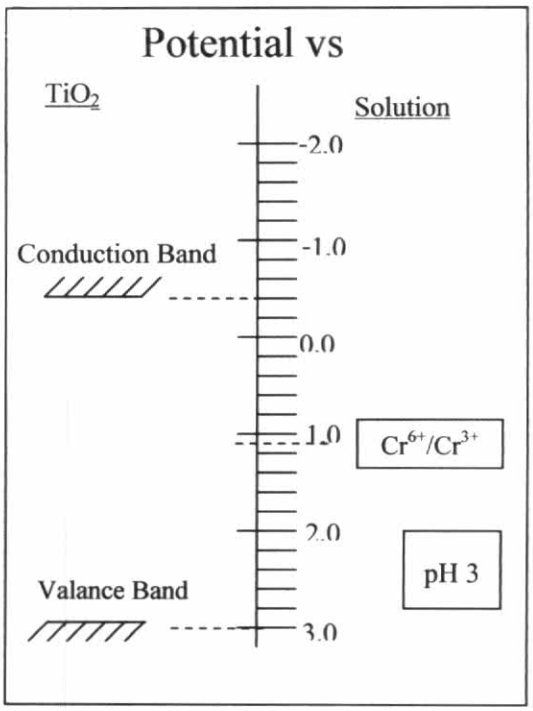

Figure 2.15 Relative disposition of the conduction and valence band-edges in TiO_2 and the redox energy levels for relevant species of chromium in an aqueous medium at pH 3. (Chen, 2001)

2.5.1.3 Photocatalytic reaction of TiO_2 nanotube array

A recent innovation in photocatalysis using TiO_2 nanotube arrays has been study, TiO_2 nanotube array film is expected to be a promising photocatalyst to overcome such drawbacks due to its great specific surface area. Moreover, the TiO_2 nanotube array film possesses a very strong mechanical strength, because it grows directly on the titanium substrate by electrochemical anodic oxidation method, which is verified to be a relatively simple and efficient process for fabricating the nanostructured TiO_2 films. Additionally the conductive support substrate is able to exhibit some interesting properties of photoelectrocatalytic and photoelectrochemistry (Quan *et al.*, 2007).

TiO_2 nanotube arrays have high efficient to exhibit increased a higher photoelectrocatalytic capability when compared with a traditional TiO_2 film electrode fabricated using the anodization method for pentachlorophenol (PCP) degradation in

aqueous solution. The study influence the photoelectrocatalytic behaviour of TiO_2 nanotubes such as the bias potential, pH value, and electrolyte concentration were shown to be important factor the degradation of PCP by photoelectrocatalytic (Quan *et al.*, 2007) had also investigated large arrays of oriented TiO_2-based nanotubes and continuous films by thermal treatment method. The photoelectrocatalytic degradation of PCP in Na_2SO_4 aqueous solution over the nanotube-like anatase TiO_2 electrode was investigated. In addition, factors affecting pphotoelectrochemical processes, i.e., applied bias potential, light intensity, concentration of electrolyte, and pH value were studied, the result show new prepared type of photoelectrode, a TiO_2 nanotube electrode, first by a sol–gel method and then by treatment to form the tubular structure in NaOH aqueous solution have the kinetic constant of PEC degradation of PCP using TiO_2 nanotubes electrode is 75% higher than that using TiO_2 film electrode. Using a photoelectrocatalytic process, PCP can be degraded completely and mineralized for a photoelectrocatalytic process in the desired time. In the present study, PCP molecules were believed to adsorb on electrode and were excited by irradiation to produce more activated PCP molecules for electrochemical degradation, and external potential bias, pH, and electrolytes are three major factors affecting the degradation of PCP in the photoelectrocatalytic process. This technique may be useful to treat organic species with low concentration.

Recently Zhuang *et al.* (2007) study on the influences of the thickness of the nanotube array film and diameters of nanotubes in photocatalytic activity using methyl oranges as the probe substance, the experiment results indicated the behaviour of the TiO_2 nanotube film depend on the structures of the nanotube array. The nanotube array films exhibited a drastically compared with the TiO_2 nanoparticles film prepared by the sol-gel method. The film thickness markly influenced the photocatalysis. However, for a given nanotube length, the tube diameter was only very slightly affected the photocatalysis efficiency.

Tian *et al.* (2003) firstly prepared and characterized the anatase TiO_2-based nanotubes films by thermal treatment method, yet but they did not test their application in environment. Lai *et al.* (2006) have also reported effects of the crystallographic structure and porous size of TiO_2 nanotube array on photocatalytic activity, the methylene blue (MB) aqueous solution were evaluated. The results

shown the photocatalytic activity of the titanium dioxide nanotube array was strongly dependent on the anodization voltage at 20 V and calcinations temperature at 450 °C due to increase in the anatase crystal phase and an increase surface area. When the calcination temperature was higher than 450 °C, the photocatalytic activity of the TiO_2 nanotube decreased, which was ascribed to excessive retile content and decrease in surface area, and initial concentration, pH in aqueous solution were show to be important factor influencing the degradation organic by using the TiO_2 nanotube film electrode as the semiconductor.

2.5.2 Dye sensitized TiO_2 nanotube arrays for DSSC applications

Dye sensitized solar cells (DSSC) have attracted attention for conversion of solar energy to electric power as a low-cost alternative to conventional solid-state photovoltaic devices (Bach *et al.*, 1998). Dye-sensitization has also recently been recognized as an important process in photon harvesting from visible light, and intense scientific studies of the photon-to-electron conversion have been undertaken with a view to the photochemical and photoelectrical conversion of solar light using wide-bandgap metal oxides with ZnO, SnO_2, TiO_2 and $SrTiO_3$ as semiconductors, and chlorophylls, cyanine dyes, xanthenes dyes, azo dyes and metal complexes such as ruthenium trisbipyridine complexes, such as Ru(bpy) (bpy=2,2- bipyridine) as sensitizing dye. Consequently, a wide variety of dyes with differing binding groups and linkers have been tested as photosensitizes in the Grätzel cell. Anchoring to semiconductor has been achieved through a number of functional groups, such as salicylate, carboxylic acid, sulphonic acid, phosphonic acid and acetylacetonate derivatives, the most widely used and successful to date being the carboxylic acid and phosphonic acid functionalities. The carboxylic acid groups, while ensuring efficient adsorption of the dye on the surface also promote electronic coupling between the donor levels of the excited chromophore and the acceptor levels of the TiO_2 semiconductor (Campbell *et al.*, 2004).

2.5.2.1 Mechanism of the dye sensitized solar cell

A typical cell is composed of two layers of Indium tin oxide coated glass (ITO), one of which is coated with TiO_2 sandwiched together with a suitable electrolyte and counter electrode. The conventional electrolyte used in this process in and iodine/iodide complex and the counter electrode is simply an $InSnO_2$ glass slide coated with a thin layer of graphite carbon. A typical setup of dye sensitized solar cell is shown in figure 2.16 below.

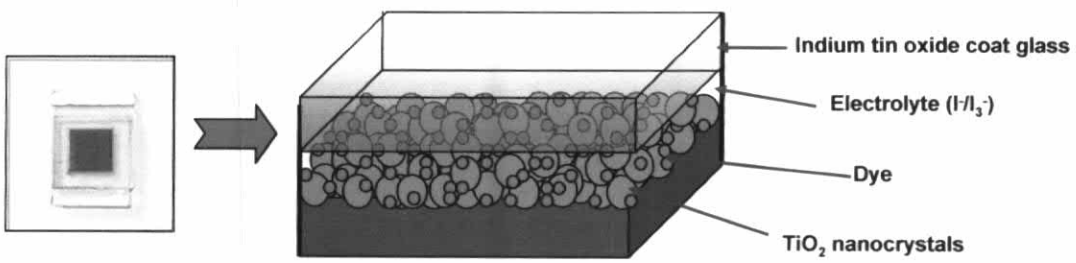

Figure 2.16 Configuration of TiO_2 dye sensitized solar cell

The cell operates on a process that is similar in many respects to photosynthesis, the process by which green plants generate chemical energy from sunlight. The cell consists of a dye-adsorbed mesoporous metal-oxide film filled with iodide/triiodide redox electrolyte and a Pt counter electrode. The system is a mesoscopic semiconductor oxide film, which is placed in contact with a redox electrolyte or an organic hole conductor. The material of choice has been TiO_2 (anatase), although alternative wide-band-gap oxides such as ZnO and Nb_2O_5 have also been investigated. Attached to the surface of the nanocrystalline film is a monolayer of the sensitizer. Photoexcitation of the latter results in the injection of an electron into the conduction band of the oxide. The dye is regenerated by electron donation from the electrolyte, usually an organic solvent containing a redox system, such as the iodide/triiodide couple. The regeneration of the sensitizer by iodide intercepts the recapture of the conduction band electron by the oxidized dye. The iodide is regenerated, in turn, by the reduction of triiodide at the counter electrode, with the circuit being completed via electron migration through the external load. The voltage generated under illumination corresponds to the difference between the Fermi

level of the electron in the solid and the redox potential of the electrolyte. Overall, the device generates electric power from light without suffering any permanent chemical transformation (Grätzel; 2003). Schematic of operational diagram of dye sensitized TiO_2 nanocrystals as light harvesting unit was shown in Figure 2.17.

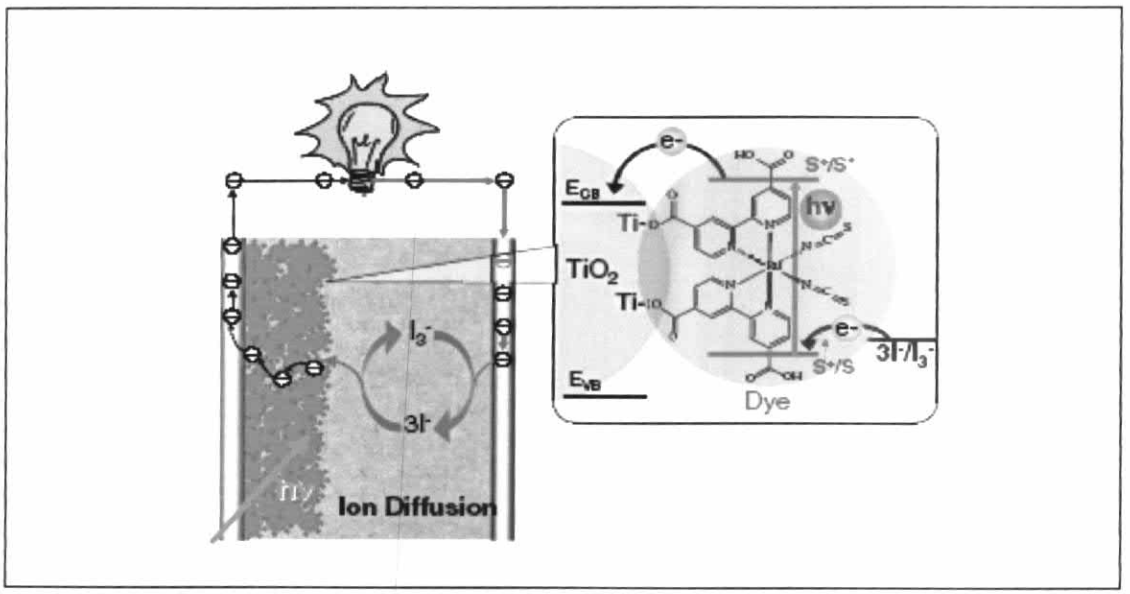

Figure 2.17 Schematic of the currently used embodiment of the dye sensitized cell. It employs dye-dervatized TiO_2 nanocrystals as light harvesting unit.

2.5.2.2 Highly-ordered TiO_2 nanotubes arrays in the DSSC

When the dye-sensitized nanocrystalline solar cell was first presented perhaps the most puzzling phenomenon was the highly efficient charge transport through the nanocrystalline TiO_2 layer. The mesoporous metal-oxide film with a large surface area plays a crucial role for the high performance of DSSCs (Barbe *et al.*, 1997; Kalyanasundaram *et al.*, 1998; Zukalova *et al.*, 2005). It not only adsorbs a large number of dye molecules for efficient light-harvesting, but also serves as a semiconductor to provide a pathway for electron percolating through the film. The crystalline structure of the metal-oxide semiconductor significantly affects the transport efficiency of the injected electron due to the structural disorder at the contact between two crystalline nanoparticles lead to enhanced scattering of free electrons, thus reducing electron mobility (Peng *et al.*, 2003). Electron transport is a limiting factor in the performance of these nanoporous nanocrystalline electrodes, hindering

progress in achieving higher efficiencies. because (a) the inherent conductivity of the film is very low; (b) the small size of the nanocrystalline particles dose not support a built-in electrical field; (c) the electrolyte penetrates the porous film all the way to the back-contact marking the semiconductor/electrolyte interface essentially three-dimentional (Gratzel, 2003). Moreover the collection of photoinjected electrons competes with recombination, a high charge-collection efficiency requires that transport is significantly faster than recombination (Van de Lagemaat *et al.*, 2000; Benkstein *et al.*, 2003; Wang *et al.*, 2001; Peter *et al.*, 2002; Katoh *et al.*, 2004; Adachi *et al.*, 2004; and Jiu *et al.*, 2005). Films constructed of oriented one-dimensional nanostructure, such as nanotube arrays aligned perpendicular structure permits vectorial charge transfer from the solution to the collecting conducting oxide substrate, thereby reducing the losses incurred by charge-hopping across nanoparticles grain boundaries (Grätzel, 2004; Adachi *et al.*, 2003). Several nanotubular architectures have been investigated for potential enhancement of electron percolation pathways and light conversion as well as improved ion diffusion at the semiconductor-electrolyte interface.

2.5.2.3 Porphyrins as light harvesting dyes in the DSSC

The most successful DSSC is the commonly known Grätzel cell, using Ru-polypyridyl based dyes adsorbed on nanocrystalline films of titanium dioxide (Nazeeruddin *et al.*, 2001). Optimally, a dye for a DSSC should absorb across the entire visible spectrum, bind strongly to the semiconductor surface, have a suitably high redox potential for regeneration following excitation and be stable over many years of exposure to sunlight. The Ru-polypyridyl complexes utilised by Grätzel come close to fulfilling these requirements, the photochemical properties of ruthenium bipyridyl dyes have attracted interest for a wide range of applications due to their strong visible absorption bands, long-lived excited state, and excellent photochemical stability. However, an important drawback of the ruthenium-based sensitizers is their lack of absorption in the red region of the visible spectrum. In addition, ruthenium complexes are likely to become increasingly more expensive as the demand for Ru raw materials increase. Interesting candidates absorbing in the 500-700 nm range are porphyrins and phthalocyanines because of their Q absorption

bands and therefore they are promising candidates for better harvesting of the solar spectrum. Several groups have reported porphyrins and phthalocyanines as sensitizers for wide-band gap oxide semiconductors (He *et al.*, 2001; He *et al.*, 2002) but in all these cases, the conversion efficiency was quite low. At least two factors play a role in this regard: one is the tendency of phthalocyanines and porphyrins to form aggregates and the other is the lack of directionality in the injection of electrons from the dye excited state to the semiconductor.

2.5.2.4 Porphyrins dye for TiO_2 sensitization

The use of porphyrins as light harvesters on semiconductors is particularly attractive given their primary role in photosynthesis and the relative ease with which a variety of covalent or noncovalent porphyrin arrays can be constructed. The attachment of a large porphyrin array to a nanocrystalline semiconductor surface provides a way to dramatically increase the surface dye concentration and therefore, the light energy conversion efficiency of the device. Various porphyrins have been used for the photosensitization of wide-band-gap semiconductors like NiO, ZnO and TiO_2, the most common being the free-base and zinc derivatives of the *meso*-benzoic acid substituted porphyrin TCPP (Figure 2.18).

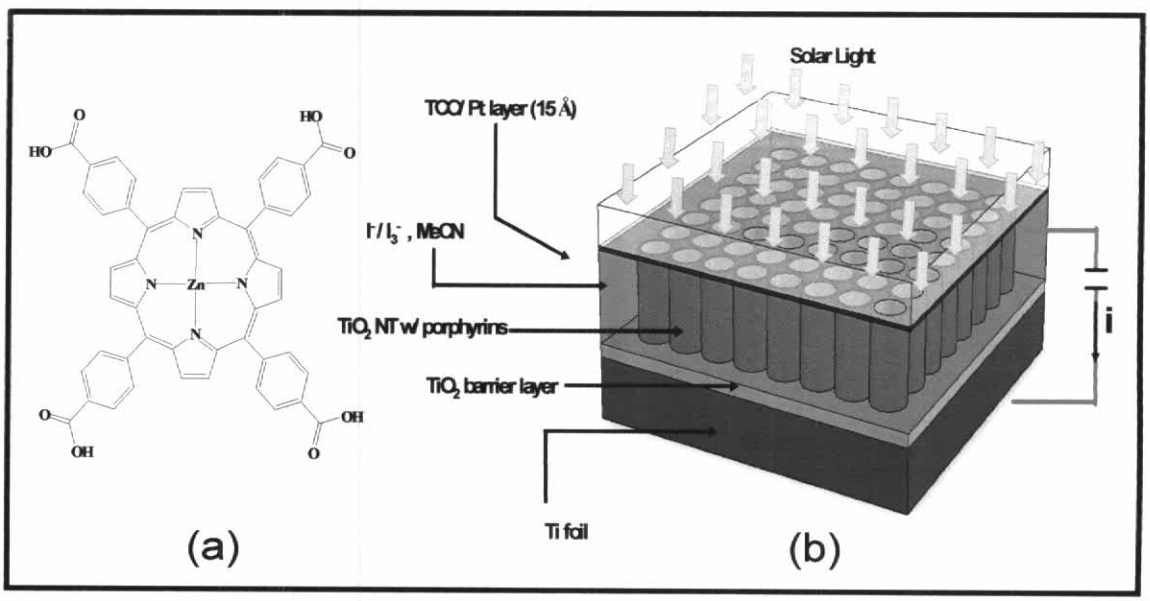

Figure 2.18 Schematic representation of porphyrin sensitized TiO_2 nanotube arrays containing DSSC device. Illumination is done through the TCO glass coated with a transparent Pt layer (15 Å).

These porphyrins exhibit long-lived (>1 ns) π^* singlet excited states and only weak singlet/triplet mixing. They have an appropriate LUMO level that resides above the conduction band of the TiO_2 and a HOMO level that lies below the redox couple in the electrolyte solution, required for charge separation at the semiconductor/dye/electrolyte surface. The relative LUMO and HOMO energy levels have been estimated for a range of dyes including TCPP, Zn-TCPP and N3 bound to TiO_2 using a new UV photoemission yield technique (Ma *et al.*, 2002). Both Grätzel and co-workers (Kalyanasundaram *et al.*, 1987) and Fox and co-workers (Dabestani *et al.*, 1988) have reported efficient charge injection from the excited state of Zn-TCPP into the conduction band of TiO_2 ($IPCE_{Soret}$ = 42%, IPCEQ band = 8–10%) and ($IPCE_{Soret}$ = 9.5%, $I_{sc} \approx 2.5$ μAcm^{-2}), respectively, however no AM 1.5 normalised cell efficiencies were stated. Boschloo and Goossens (1996) photosensitised TiO_2 with Zn-TCPP, giving a low η of 1.1% ($IPCE_{Soret}$ = 40%, $IPCE_{Q\ band} \approx$ 10–16%, V_{oc} = 0.36 V, I_{sc} = 0.85 $mAcm^{-2}$). A more recent and promising result is that from Cherian and Wamser (2000) whose TCPP-based TiO_2 photovoltaic cells gave good solar-energy conversion efficiencies under AM 1.5 conditions (η = 3.5%, fill factor of 62%, $IPCE_{Soret}$ = 55%, $IPCE_{Q\ band}$ = 25–45%, V_{oc} = 485 mV, I_{sc} = 6 $mAcm^{-2}$). To date this is the best-reported value for a porphyrin PEC, and was achieved using deoxycholic acid (DCA) as a co-adsorbate. Wamser (2003) have also reported a solid state based Grätzel cell, which uses aminophenyltricarboxyphenylporphyrin dye TC3APP with an aniline gel-based electrolyte system, giving an η value of 0.8%. Recently, Durrant and co-workers (Tachibana *et al.*, 2000) compared the electron injection and charge recombination of N3, free-base TCPP and Zn-TCPP on TiO_2. Their studies show that these three dyes have almost indistinguishable electron injection and recombination kinetics. They state that the high efficiency reported for N3 dye probably originates from differences in the rate of electron transfer to the dye cation from the iodide redox couple used in these devices. It is also possible that the lower efficiency of porphyrin sensitizers results from the increased probability of exciton annihilation from close porphyrin proximity. Porphyrins have a inherent tendency to aggregate (Viseu *et al.*, 2002), and at high dye coverage, dipole/dipole interactions are expected to allow rapid migration of the excited state between neighbouring dyes, increasing the probability of excision annihilation. Odobel *et al.* (2003) are currently investigating a range of region isomers of *meso*-substituted phosphonic acid functionalised porphyrins. They

claim that the nature of the functional group has little impact on the DSSC performance, but the position of substitution (*meta*, *para*) has a greater influence. They have also compared derivatives containing carboxylic acid TCPP, sulphonic acid TSPP and TPP in the DSSC. Their results indicate that the binding state and the amount of dye adsorbed are all important factors in DSSC performance.

Very recently, a near-IR absorbing zinc phthalocyanine was reported with excellent conversion of light to electric power when adsorbed on nanocrystalline TiO_2 films (Reddy *et al.*, 2007). The rationale behind the good performance of this newly synthesized phthalocyanine is based on the incorporation of *tert*-butyl groups in combination with anchoring carboxylic acid groups which exert a "push-pull" effect promoting directionality in the dye electronic orbitals toward the semiconductor substrate (Reddy *et al.*, 2007). This directionality affords an efficient electron transfer pathway from the excited dye to the TiO_2 conduction band. For tetrachelate porphyrin chromophores bound to metal oxide (TiO_2 or ZnO) nanoparticulate films, the effect of spacer length and anchoring group position on the binding geometry, and as a result, on the photoelectrochemical properties, was recently reported by Rochford *et al.* (2007) The binding geometry was found to dramatically influence the photoelectrochemical efficiency which in the best cases, reached IPCE values of ~57% at 430 nm (Soret band), 34% at 570 nm, and 21% at 600 nm (i.e., at the porphyrin Q bands). This good performance was associated with a planar absorber configuration and individual adsorption through short rigid linkers on the oxide surface whereas other porphyrins either with longer linkers or with tendency to aggregate on the oxide surface showed a significantly lower performance.